

On the scalar probability density function transport equation for binary mixing in isotropic turbulence at supercritical pressure

Hong Lou and Richard S. Miller^{a)}

Department of Mechanical Engineering, Clemson University, Clemson, South Carolina 29634-0921

(Received 9 April 2001; accepted 22 August 2001)

Effects of Soret cross-diffusion, whereby concentration diffusion occurs in the presence of either temperature or pressure gradients, are investigated in the context of the binary isotropic turbulent mixing problem at supercritical pressure with emphasis on results relevant to probability density function (PDF) modeling. Direct numerical simulations (DNS) are conducted for compressible isotropic turbulent binary mixing of heptane with nitrogen at mean pressure and temperature equal to 45 atm and $T=700$ K, respectively. The formulation is based on a cubic real gas state equation, and includes generalized forms for heat and mass diffusion derived from nonequilibrium thermodynamics and fluctuation theory. Results from two simulations at 192^3 resolution are compared. One case is based on the complete diffusion formulation, whereas in the second simulation only “standard” Fickian and Fourier mass and heat flux terms are considered as a basis for comparisons. The evolutions of the two mixing processes are shown to be nearly the same at early times; however, at long times the pressure gradient based Soret diffusion acts as a forcing function resulting in a statistically stationary scalar fluctuation distribution. In this case the scalar variance achieves a stationary value, in contrast to the exponential decay associated with purely Fickian diffusion. The mechanical to scalar time scale ratio, $C_Y = \tau_u / \tau_Y$, is increased by a factor of approximately 3 by Soret effects during this latter mixing regime. Soret diffusion is shown to substantially alter the forms of the conditional expected diffusion and the conditional expected dissipation at these long times. A commonly used model based on an assumed proportionality between the conditional diffusion and the scalar fluctuation is tested, and is found to perform poorly in the presence of cross diffusion at long mixing times. Several new conditional expectations resulting from cross diffusion are measured. Implications of the results for extension of PDF models to the high pressure regime are discussed. © 2001 American Institute of Physics.
[DOI: 10.1063/1.1410125]

I. INTRODUCTION

Probability density function (PDF) methods¹ have received widespread attention in the literature, having been applied to reacting flows,^{1,2} inhomogeneous flows,³ compressible flows,^{4,5} and multiphase flows.^{6,7} In these studies, heat and mass diffusion are nearly universally assumed to be governed by Fourier’s and Fick’s diffusion laws, respectively. Possible influences of nonequilibrium “cross-diffusion” effects, by which species diffuse due to temperature and/or pressure gradients (Soret or “thermal,” diffusion), and thermal energy diffuses due to species and/or pressure gradients (Dufour diffusion, or “diffusion-thermo”), have been ignored. This is despite the fact that these cross-diffusion effects can significantly affect the mixing process; particularly in the presence of large molecular weight ratios and for high pressure compressible flows.^{8–20} The present investigation therefore addresses the possible influence of Soret (and Dufour) diffusion in the context of PDF methods for the case of binary hydrocarbon mixing in compressible isotropic turbulence under supercritical pressure conditions.

PDF methods have been applied to the simulation of turbulent flows for more than 30 years.^{1,2,21–26} In this class of models, a transport equation is solved for the evolution of the single-point, single-time joint scalar, or joint velocity-scalar, PDF. The primary advantage of PDF methods for combustion modeling lies in the fact that chemical reaction source terms appear in closed form and therefore do not require modeling.¹ In contrast to Reynolds averaged based turbulence models, modeling requirements are shifted to terms involving molecular mixing. Due to the nature of this closure problem, the relatively simple case of binary mixing in incompressible isotropic turbulence has been widely used as a model flow for studying unclosed mixing terms and closure models. In this case, the exact PDF transport equation for the conserved scalar mass fraction (Y) of either species can be expressed in either of the two consistent forms:¹

$$\rho \frac{\partial f}{\partial t} = \frac{\partial^2}{\partial \psi^2} \left[\left\langle J_j \frac{\partial Y}{\partial x_j} \middle| \psi \right\rangle f \right], \quad (1)$$

$$\rho \frac{\partial f}{\partial t} = \frac{\partial}{\partial \psi} \left[\left\langle \frac{\partial J_j}{\partial x_j} \middle| \psi \right\rangle f \right], \quad (2)$$

where $f(Y)$ is the PDF of scalar Y , ρ is the (constant) density, J_j is the diffusion flux vector, and the bracketed terms ap-

^{a)}Electronic mail: rm@clemson.edu

pearing on the right-hand sides of the equations indicate averages conditioned on the scalar taking values $Y = \psi$. The scalar mass diffusion vector is generally assumed to obey Fick's law; $J_j = -\rho D \partial Y / \partial x_j$, where D is the binary diffusion coefficient.

The conditional averages appearing in Eqs. (1) and (2) are referred to as the "conditional expected scalar dissipation" and the "conditional expected scalar diffusion," respectively. The mean scalar dissipation is related to the conditional expected dissipation by

$$\epsilon_Y = - \int_{-\infty}^{+\infty} \left\langle J_j \frac{\partial Y}{\partial x_j} \middle| \psi \right\rangle f d\psi, \quad (3)$$

which can be simplified for Fickian diffusion in terms of an ensemble average:

$$\epsilon_Y = \left\langle \rho D \frac{\partial Y}{\partial x_j} \frac{\partial Y}{\partial x_j} \right\rangle. \quad (4)$$

In this case, ϵ_Y is restricted to non-negative values consistent with its dissipative role in the scalar variance transport equation:

$$\rho \frac{d}{dt} \left[\frac{\langle Y' Y' \rangle}{2} \right] = \left\langle J_j \frac{\partial Y}{\partial x_j} \right\rangle = -\epsilon_Y, \quad (5)$$

where the superscript ' indicates a fluctuation with respect to the mean; i.e., $Y = \langle Y \rangle + Y'$. Note that the expected value of the scalar diffusion is null due to homogeneity. Both forms of the conditional expectations are unclosed in the context of PDF methods, and one or the other requires modeling.

A large body of research has appeared in the literature addressing the binary mixing problem described above. The extent of this literature relating to both the measurement and modeling of the conditional scalar expectations is too large to review in this paper. However, it is generally accepted that a successful model for either of the conditional expectations will accurately reproduce observed decay of the scalar PDF from its initial "double delta" form (nonpremixed) to an asymptotically gaussian state (well mixed).^{27,28} It should be noted that evidence also exists for asymptotically non-gaussian forms of the scalar PDF characterized by "exponential tails,"²⁹⁻³¹ with direct impact on the corresponding forms of the conditional scalar expectations. These observations have inspired substantial interest in the measurement and modeling of conditional scalar statistics in turbulent flows. The scalar variance is further assumed to exhibit an approximately exponential decay, and several mixing models applicable to PDF methods are based on this assumption.

The above review of PDF methods has only considered the case of Fickian mass diffusion. However, in its general form, the mass flux vector J_i for the binary mixing problem can be decomposed into three separate flux vectors:¹⁹ $J_i = J_i^Y + J_i^T + J_i^P$, where the superscript indicates the thermodynamic gradient involved; i.e., $J_i^Y = -C^Y \partial Y / \partial x_j$, $J_i^T = -C^T \partial T / \partial x_j$, and $J_i^P = -C^P \partial P / \partial x_j$, where T is the temperature, P is the pressure, and C^Y , C^T , and C^P are appropriately defined thermodynamic functions (see below) which can be derived from nonequilibrium thermodynamics and

fluctuation theory.³² Substituting this decomposition of the mass flux vector into the PDF transport equation yields

$$\rho \frac{\partial f}{\partial t} = \frac{\partial^2}{\partial \psi^2} \left[\left\langle \left\langle J_j^Y \frac{\partial Y}{\partial x_j} \middle| \psi \right\rangle \right\rangle + \left\langle \left\langle J_j^T \frac{\partial Y}{\partial x_j} \middle| \psi \right\rangle \right\rangle + \left\langle \left\langle J_j^P \frac{\partial Y}{\partial x_j} \middle| \psi \right\rangle \right\rangle \right] f \quad (6)$$

or

$$\rho \frac{\partial f}{\partial t} = \frac{\partial}{\partial \psi} \left[\left\langle \left\langle \frac{\partial J_j^Y}{\partial x_j} \middle| \psi \right\rangle \right\rangle + \left\langle \left\langle \frac{\partial J_j^T}{\partial x_j} \middle| \psi \right\rangle \right\rangle + \left\langle \left\langle \frac{\partial J_j^P}{\partial x_j} \middle| \psi \right\rangle \right\rangle \right] f. \quad (7)$$

Note that it is only the Fickian flux J_i^Y which contributes to the true scalar dissipation¹⁹ (discussed below) and should therefore be related to the mass flux appearing in Eqs. (1)–(5). The relatively unexplored influence of the cross diffusion fluxes J_i^T and J_i^P on the above relations are to be determined.

Miller¹⁹ conducted direct numerical simulations (DNS) of hydrocarbon–nitrogen mixtures in stationary isotropic compressible box turbulence at supercritical pressure, with a formulation which includes generalized diffusion and a real gas state equation. It was shown that initially perfectly premixed binary species will "anti-diffuse" due to the presence of temperature and pressure fluctuations in the flow and their corresponding influence on the cross diffusion fluxes J_i^T and J_i^P . This was explained in the context of the scalar variance transport equation for the species mass fraction:

$$\frac{d}{dt} \left[\langle \rho \rangle \frac{\langle \langle Y'' Y'' \rangle \rangle}{2} \right] = \left\langle \left\langle J_j^Y \frac{\partial Y}{\partial x_j} \right\rangle \right\rangle + \left\langle \left\langle J_j^T \frac{\partial Y}{\partial x_j} \right\rangle \right\rangle + \left\langle \left\langle J_j^P \frac{\partial Y}{\partial x_j} \right\rangle \right\rangle, \quad (8)$$

where the double brackets indicate the mass weighted Favre average, and $Y = \langle \langle Y \rangle \rangle + Y''$. As mentioned above, only the first term on the right-hand side can be interpreted as a true (non-negative) dissipation term:

$$\epsilon_Y = - \left\langle \left\langle J_j^Y \frac{\partial Y}{\partial x_j} \right\rangle \right\rangle. \quad (9)$$

Miller¹⁹ observed that a statistical balance is achieved between this Fickian dissipation term and variance production primarily attributed to the pressure gradient induced Soret term containing J_i^P . These competing processes result in a highly skewed non-Gaussian scalar PDF with stationary variance at long times. It was observed that the magnitude of the long time scalar variance increases with increasing turbulence Mach number and molecular weight ratio, as well as with decreasing turbulence Reynolds number. It was also noted that the stationary long time scalar distribution is inconsistent with the accepted exponential scalar variance decay in typical (low pressure) nonpremixed studies.

The primary objective of the present paper is to extend the DNS of Miller¹⁹ to the case of binary nitrogen–hydrocarbon mixing of initially segregated species at supercritical pressure, and to analyze the results in the context of scalar distribution evolutions and conditional statistics relevant to PDF methods. The paper is organized as follows. The formulation and numerical approach are summarized in Sec. II. Results from two simulations at resolutions of 192³

grid points are presented in Sec. III. In one case the full generalized diffusion fluxes are included in the formulation. The second simulation has identical parameters; however, only the traditional Fickian and Fourier diffusion terms are considered in order to analyze the influence of cross-diffusion on the mixing process. Conclusions and further discussions are presented in Sec. IV.

II. FORMULATION AND NUMERICAL APPROACH

The formulation and the numerical approach for the supercritical binary mixing problem under consideration have already been described in detail in Ref. 19 and are therefore only summarized in what follows.

A. Conservation equations for binary mixture

For pressures higher than the thermodynamic critical point (the critical “locus” for mixtures) the distinction between gaseous and liquid phases vanishes, and deviations from ideal gas behavior become significant.³³ The following formulation therefore includes conservation equations for a single phase fluid mixture density, momentum, total energy (internal plus kinetic), and species mass fraction, as well as a real gas state equation (the cubic Peng–Robinson state equation is chosen for the present study):

$$\frac{\partial \rho}{\partial t} + \frac{\partial}{\partial x_j} [\rho u_j] = 0, \quad (10)$$

$$\frac{\partial}{\partial t} (\rho u_i) + \frac{\partial}{\partial x_j} [\rho u_i u_j + P \delta_{ij} - \tau_{ij}] = \rho F_i, \quad (11)$$

$$\frac{\partial}{\partial t} (\rho e_t) + \frac{\partial}{\partial x_j} [(\rho e_t + P) u_j - u_i \tau_{ij} + Q_j] = \rho u_i F_i, \quad (12)$$

$$\frac{\partial}{\partial t} (\rho Y_B) + \frac{\partial}{\partial x_j} [\rho Y_B u_j + J_j] = 0, \quad (13)$$

$$P = \frac{RT}{V - B_m} - \frac{A_m}{V^2 + 2VB_m - B_m^2}. \quad (14)$$

In the above expressions, u_i is the velocity vector, τ_{ij} is the Newtonian viscous stress tensor, δ_{ij} is the Kronecker delta tensor, F_i is an artificial “stirring” force added to maintain statistically stationary turbulence, e_t is the specific total energy, and Q_i is the heat flux vector. A binary mixture comprised of components denoted as species A and species B is considered. In this case only a single transport equation for the mass fraction of species B (Y_B) is included in the formulation, while the corresponding mass fraction of species A is calculated as $Y_A = 1 - Y_B$. The mass flux vector for species B is denoted J_i , while conservation of mass requires that the mass flux for species A is $-J_i$. Finally, A_m and B_m are mixture parameters for the state equation which are defined based on appropriately chosen mixing rules.³³

B. Heat and mass flux vectors

General expressions for the forms of the heat and mass flux vectors can be derived based on Keizer’s fluctuation–dissipation theory,³⁴ combined with nonequilibrium

thermodynamics,³² by assuming that each flux vector is linearly proportional to gradients of both the thermal and chemical potentials. As a matter of convenience, Miller¹⁹ presented these fluxes as a superposition of separate flux vectors relating to gradients of the mass fraction, temperature, and pressure: $Q_j = Q_j^T + Q_j^Y + Q_j^P$, and $J_j = J_j^T + J_j^Y + J_j^P$, defined as follows:

$$Q_j^T = - \left\{ \kappa + \rho D \alpha_{\text{IK}} \alpha_{\text{BK}} Y_A Y_B R \left(\frac{M_m}{M_A M_B} \right) \right\} \frac{\partial T}{\partial x_j}, \quad (15)$$

$$Q_j^Y = - \left\{ \rho D \alpha_d \alpha_{\text{IK}} R T \left(\frac{M_m}{M_A M_B} \right) \right\} \frac{\partial Y_B}{\partial x_j}, \quad (16)$$

$$Q_j^P = - \left\{ \rho D \alpha_{\text{IK}} Y_A Y_B \left(\frac{V_{,B}}{M_B} - \frac{V_{,A}}{M_A} \right) \right\} \frac{\partial P}{\partial x_j}, \quad (17)$$

$$J_j^T = - \left\{ \rho D \alpha_{\text{BK}} \frac{Y_A Y_B}{T} \right\} \frac{\partial T}{\partial x_j}, \quad (18)$$

$$J_j^Y = - \left\{ \rho D \alpha_d \right\} \frac{\partial Y_B}{\partial x_j}, \quad (19)$$

$$J_j^P = - \left\{ \rho D \frac{Y_A Y_B}{RT} \left(\frac{M_A M_B}{M_m} \right) \left(\frac{V_{,B}}{M_B} - \frac{V_{,A}}{M_A} \right) \right\} \frac{\partial P}{\partial x_j}. \quad (20)$$

In the above expressions, κ is the form of the thermal conductivity consistent with kinetic theory, R is the universal gas constant, M_α is the molecular weight of species α (subscript m indicates the mixture value), and $V_{,\alpha}$ is the partial molar volume of species α .

Three additional thermodynamic relations appear in the above expressions. The parameters α_{IK} and α_{BK} are referred to as the “Irving–Kirkwood” and the “Bearman–Kirkwood” forms of the thermal diffusion factor,^{35,36} respectively. These two factors are related to one another through an expression derived by Harstad and Bellan:¹⁸

$$\alpha_{\text{IK}} = \alpha_{\text{BK}} + \frac{1}{RT} \left(\frac{M_A M_B}{M_m} \right) \left(\frac{H_{,B}}{M_B} - \frac{H_{,A}}{M_A} \right), \quad (21)$$

where $H_{,\alpha}$ is the partial molar enthalpy of species α . Equation (21) implies that only one of these parameters needs to be specified based on the specific species under consideration; the other is then known implicitly through the above equation. Finally, the mass diffusion factor α_d is related to molar gradients of the fugacity; its form can be derived given a specific equation of state. Under “normal” low pressure conditions, $\alpha_d \approx 1$, thereby recovering the Fickian form of the mass diffusion term J_i^Y in Eq. (19). In contrast, $\alpha_d \rightarrow 0$ along the critical locus of the state equation.

The reader is referred to Ref. 19 for additional details of the formulation. These include the specific mixing rules used for the state equation, as well as expressions for the mixture mass diffusion factor, internal energy, heat capacity, partial molar volume, and partial molar enthalpy (all of which are derived from the Peng–Robinson state equation for consistency).

C. Numerical approach

The above equations are solved for the case of isotropic box turbulence in a triply periodic domain having equal lengths L in each of the three coordinate directions; x_1 , x_2 , and x_3 . Statistically stationary turbulent flow is maintained via the addition of an artificial forcing term added to the momentum and energy equations having a form originally proposed by Kida and Orszag.³⁷ The governing equations are solved using a third order Runge–Kutta time advancement procedure coupled with eighth order accurate central finite differencing for all spatial derivatives.³⁸ Tenth order accurate explicit filtering is applied to the primitive variables at each Runge–Kutta stage to control numerical oscillations in the solution. Additional details relating to the numerical methodology as well as to code validation can be found in Ref. 19.

D. Species properties

The binary mixing of initially segregated heptane in nitrogen is chosen as having a representative molecular weight ratio leading to significant Soret diffusion effects.¹⁹ Denoting species A to be the nitrogen, and species B to be the heptane; $M_A = 28.013$ and $M_B = 100.205$. The corresponding critical temperatures and pressures are: $T_A^C = 126.6$ K, $T_B^C = 540.3$ K, $P_A^C = 33.46$ atm, and $P_B^C = 27.04$ atm.³³ Following the molecular weight ratio based correlation provided in Ref. 14 the Irving–Kirkwood form of the thermal diffusion factor is taken to be $\alpha_{IK} = 0.1612$. This value is consistent with the choice of thermal diffusion factor shown to yield good comparisons with experimental data for supercritical heptane spherical droplet vaporization in nitrogen in Ref. 18. Diffusive properties are modeled in a simplified manner and are assumed to be species independent. The mixture viscosity (μ) is assumed to be constant and for convenience is calculated based on a specified value of a reference Reynolds number;³⁷ $Re_0 = \rho_0 U_0 L_0 / \mu$, based on reference values for the density, velocity, and length. For the present simulations, the reference density is set equal to the mean density in the domain ($\rho_0 = \langle \rho \rangle$), the reference velocity scale is taken equal to the acoustic velocity (a) based on the initial mean thermodynamic parameters ($U_0 = a_0$), and the reference length scale is $L_0 = L / (2\pi)$. Finally, the thermal conductivity and mass diffusivity are calculated from specified constant values of the Prandtl [$Pr = \mu / (\rho C_p \kappa)$] and Schmidt [$Sc = \mu / (\rho D)$] numbers; $Pr = Sc = 0.7$. Note also that the diffusive properties are intentionally treated in a relatively simplified manner in order to aid in isolating the effects of the Soret and Dufour terms in the heat and mass fluxes. Because of the simplification of these parameters, the species can only be considered to behave as “real” heptane and nitrogen with regard to the equation of state and to the molecular weight effects appearing in the diffusive fluxes.

III. RESULTS

Results from two simulations of the isotropic turbulent mixing problem are described in what follows. The two cases are denoted “run 1” and “run 2.” Run 1 includes the complete formulation of the generalized heat and mass fluxes

presented in the preceding section. Case run 2 is identical in every respect, except that only standard Fourier and Fickian diffusion are included in the formulation (the real gas state equation is retained). This is accomplished by nulling the cross-diffusional fluxes; $Q_i^Y = Q_i^P = J_i^T = J_i^P = 0$. In addition, the mass diffusion factor is taken to be unity, $\alpha_d = 1$, and the thermal diffusivities are also nulled, $\alpha_{IK} = \alpha_{BK} = 0$. These values have the effect of reducing the mass flux J_i^Y and the heat flux Q_i^T to their respective Fickian and Fourier forms. Both simulations are conducted with a resolution of 192^3 grid points, have $Re_0 = 335$, and have a nondimensional forcing amplitude equal to $F_R^* = 0.35$ (see Ref. 19).

The simulation procedure is as follows. A turbulent flow is first prepared by integrating the governing equations for a perfectly premixed, 50/50 by mass, mixture of heptane and nitrogen at initial temperature $T = 700$ K and pressure $P = 45$ atm (a_0 is based on these conditions) until a statistically stationary flow is achieved. This stationary state is characterized by mean (time averaged) fluctuating Mach number $M_C = 0.54$, and turbulence Reynolds number based on the Taylor length scale $Re_\lambda = 80.1$ (note that this is a “quasi-stationary” state for compressible flow due to viscous dissipation effects increasing the mean internal energy with time^{19,37}). The ensemble averaged (over all grid points) Mach number is defined as $M_C = \langle (u_i u_i)^{1/2} / a \rangle$ (see Ref. 19 for the calculation of the speed of sound, a). The Reynolds number is defined as $Re_\lambda = \langle \rho \rangle \langle u_i u_i \rangle [5 / (3 \mu \epsilon_u)]^{1/2}$, where the velocity dissipation is $\epsilon_u = \mu \langle \omega_i \omega_i \rangle + 4/3 \mu \langle (\partial u_i / \partial x_i)^2 \rangle$ (ω_i is the vorticity vector). The resulting stationary velocity flow field is characterized by a mean Kolmogorov length scale (η) which is larger than the grid spacing; $\eta / \Delta x = 1.18$, where $\eta = [(\mu^3 / (\epsilon_u \langle \rho \rangle^2))]^{1/4}$.

An identical realization of the stationary flow field described above is used to initialize the binary mixing problem for both cases run 1 and run 2. This is accomplished by fixing the velocity field, and re-initializing the scalar field to produce a single spherical “blob” of pure heptane fluid centered in the domain (an error function profile is used to smooth the transition gradients between the nitrogen and heptane). The terminology “blob” will be used hereinafter to describe the initial heptane configuration, since “droplet” is misleading in the absence of phase change. The diameter of the blob is chosen to retain the 50/50 mass ratio of heptane to nitrogen in the domain. Both the pressure and temperature fluctuations are maintained; however, the mean temperature is reduced by 50 K within the spherical blob to model the effects of a cold fuel spray and to enhance initial temperature gradients (and resulting cross-diffusional effects). After the new species and temperature distributions are determined, the density field is then updated to be consistent with the equation of state. The resulting segregated species flow field is then used as an initial condition for the two simulations. The forcing vector is also included for the mixing simulations in order to maintain the turbulence intensity, and to “drive” the flow towards an eventual completely mixed stationary state. All scalar and mass flux results presented hereinafter are for the heptane species (species B).

Normalized spectra as a function of the isotropic wavenumber magnitude for both the velocity and heptane mass

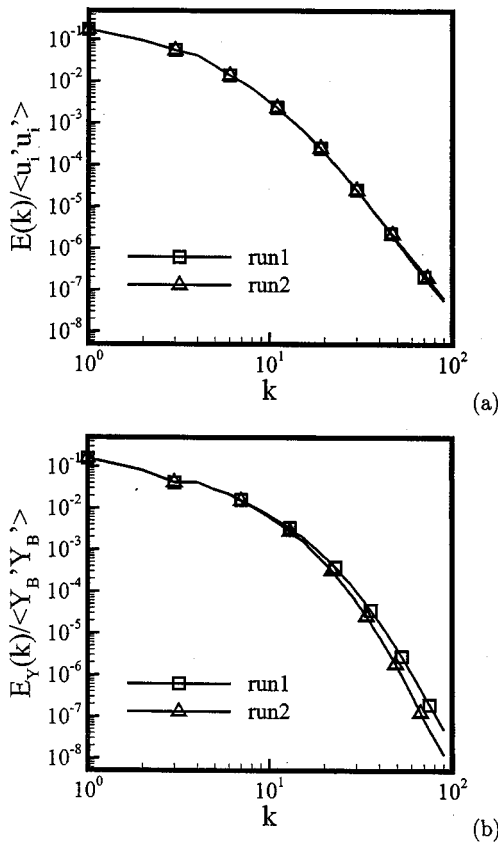


FIG. 1. Normalized spectra as a function of wavenumber magnitude at time $t^* = 5$; (a) kinetic energy and (b) heptane mass fraction.

fractions are presented at an early mixing time $t^* = 5$ (where $t^* = ta_0/L_0$ is a characteristic acoustic time scale) in Fig. 1 for simulations run 1 and run 2. The spectra reveal that the turbulence Reynolds number is not sufficiently large to result in a well-defined inertial range. However, the high wave number behavior for both the velocity and scalar fields are consistent with adequate grid resolution. Alterations in the spectral scalar behavior due to the Soret diffusion appear to be relatively minor at this time [Fig. 1(b)]. At high wave numbers the energy content is somewhat elevated in the presence of Soret diffusion (run 1). As will be shown below, this is due to the temperature gradient dependent Soret term, J_i^T , acting as a production source in the scalar variance transport equation at these times.

A qualitative description of the mixing process under consideration is provided by Fig. 2 which depicts mass flux vectors in an x_1-x_2 plane bisecting the domain ($x_3 = L/2$) at the early mixing time $t^* = 1$. At this time the spherical heptane blob, as indicated by contours of the heptane mass fraction, is just beginning to be distorted and mixed by the turbulent velocity. Mass flux vectors are shown for the total vector (J_i), as well as for each of the three subvectors due to mass fraction (J_i^Y), temperature (J_i^T), and pressure (J_i^P) gradients. At this early time cross-diffusion effects appear to be relatively minor, and $J_i \approx J_i^Y$ as observed by comparing Figs. 2(a) and 2(b). The vectors J_i^T and J_i^P in Figs. 2(c) and 2(d) have a reference length 13.3 times larger in order to illustrate the qualitative cross-diffusion behavior. The temperature gra-

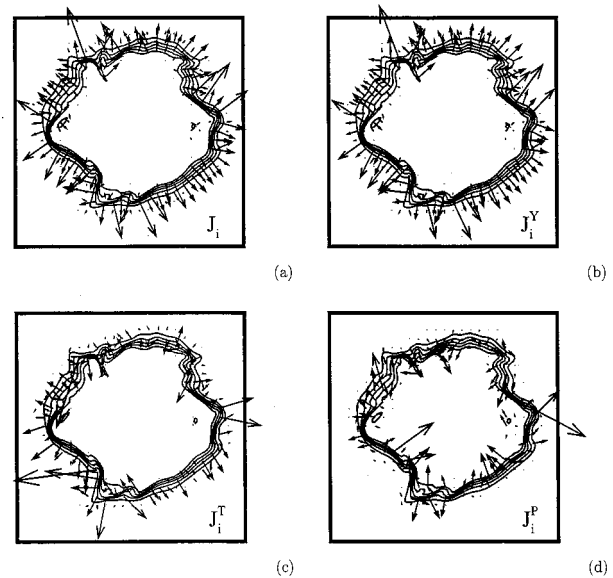


FIG. 2. Heptane mass fraction contours and mass flux vectors from simulation run 1 at time $t^* = 1$; (a) J_i , (b) J_i^Y , (c) J_i^T , and (d) J_i^P . The relative scaling of the vectors is 13.3 times larger for J_i^T and J_i^P as compared to J_i and J_i^Y . Contours are for the heptane mass fraction in increments of 0.2.

dent induced mass flux is directed predominantly out of the heptane blob; thus enhancing the total mass flux rate. This is due to the reduction of the mean temperature within the heptane blob by 50 K during initialization which produces a mean temperature gradient along the initial heptane–nitrogen boundary (superimposed on the turbulent temperature fluctuation gradient). Note that the heptane mass fraction gradient and the net temperature gradient along the boundary are anticorrelated; however α_{BK} is a negative term [see Eq. (21) and Ref. 19] resulting in the net alignment of J_i^Y and J_i^T . Note also that the direction of J_i^T is reversed for the nitrogen mass flux rate; i.e., diffusion of nitrogen into the heptane blob is enhanced by J_i^T . In contrast, the pressure field has a uniform mean and the pressure fluctuations at initialization have no correlation with the presence of the blob. This results in the more or less “random” nature of the pressure gradient induced mass flux in Fig. 2(d). This flux is directed both into and outward from the heptane region; with no obvious net contribution to the heptane egress flux.

A. Binary mixing and moment evolution

The above results for both the energy spectra and the mass flux vector visualizations appear to indicate that cross-diffusion plays a relatively insignificant role during initial stages of the mixing process. However, this is not the case at longer times. Figure 3 presents the time evolution of the heptane mass fraction minimum and maximum [Fig. 3(a)] and variance [Fig. 3(b)] for simulations run 1 and run 2. The last remnants of the intact heptane blob are destroyed by the mixing process by time $t^* \approx 12$ as evidenced by the onset of the depletion of the scalar bounds in Fig. 3(a). During the primary mixing stage $10 \leq t^* \leq 40$ the scalar bounds migrate towards the scalar mean, in this case $\langle Y \rangle = 0.5$, and only

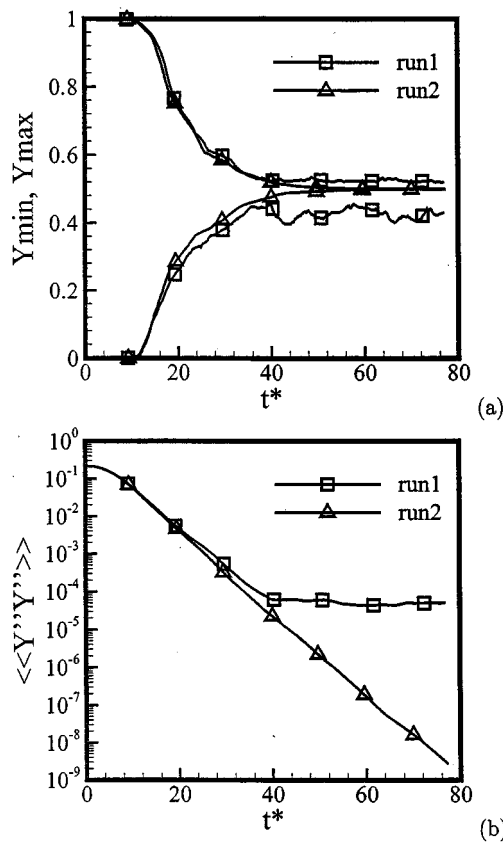


FIG. 3. Temporal evolution of heptane mass fraction (a) minimum and maximum, and (b) Favre averaged variance.

small deviations between run 1 and run 2 are apparent in either of Figs. 3(a) and 3(b). However, the latter stages of mixing are characterized by markedly different behavior when cross-diffusion effects are included. Whereas the purely Fickian diffusion in case run 2 allows for a continuous merging of the scalar bounds, the heptane mass fraction minimum and maximum do not merge when cross diffusion is present (run 1). This is further evidenced in Fig. 3(b) which shows the scalar variance evolution. Case run 2 exhibits a continuous near exponential decay of $\langle\langle Y''Y'' \rangle\rangle$. In contrast, the scalar moment for simulation run 1 decays exponentially only until $t^* \approx 40$; thereafter, a stationary scalar fluctuation state is achieved with $\langle\langle Y''Y'' \rangle\rangle \approx 5 \times 10^{-5}$.

The above mixing behavior is consistent with the stationary scalar states observed by Miller¹⁹ who studied a similar mixing process. However, in their simulations the scalar field was initialized as perfectly premixed such that the scalar bounds began both equal to 0.5. In this case, the “unmixing” of the initial scalar distributions and the eventual stationary scalar fields were explained in the context of the scalar variance evolution equation, Eq. (8). It was shown that the long time variance is characterized by a balance between dissipation from the Fickian mass flux J_i^Y , and net production effects due to the term involving the pressure gradient induced mass flux, J_i^P . The present flow involves initially non-premixed species, and the scalar variance budget evolution is correspondingly more complex.

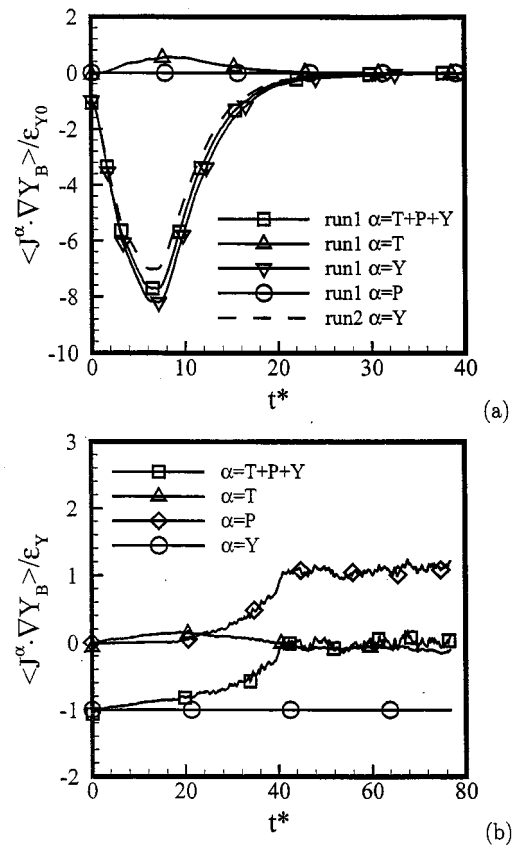


FIG. 4. Temporal evolution of the Favre averaged scalar variance budget normalized by (a) the initial dissipation and (b) the instantaneous dissipation. The results in (b) are for run 1.

Figure 4 presents the scalar variance budget [the right-hand side terms of Eq. (8)] for both run 1 and run 2 (note that only J_i^Y exists for run 2). All budget curves are normalized by the scalar variance dissipation given by Eq. (9); the normalization is based on the initial dissipation (ϵ_{Y0}) in Fig. 4(a), and by the instantaneous value in Fig. 4(b). Normalization by the initial dissipation emphasizes the early mixing process for $t^* < 40$ during which the scalar bounds and variance decay similarly for both run 1 and run 2 (see Fig. 3). For both flows the summation of terms comprising the budget variance (i.e., due to J_i) initially grow rapidly in magnitude before peaking at $t^* \approx 7$. The growth, and the following decay, of these net budget contribution magnitudes are similar for both flows.

The evolution of the variance budget depicted in Fig. 4(a) for run 1 can be explained as follows. The heptane blob is initialized with a temperature reduction of 50 K relative to the external nitrogen. A net temperature gradient is therefore present in the initial conditions which is anticorrelated with the heptane mass fraction gradient along the species boundary. The term $\langle J_i^T \partial Y_B / \partial x_j \rangle$ therefore takes negative values consistent with the negative definite dissipation term $\langle J_i^Y \partial Y_B / \partial x_j \rangle$ (recall that α_{BK} appears in the definition of J_i^T and is negative valued for the present thermodynamic conditions and species). Although difficult to discern in Fig. 4(a), the terms due to J_i^T and J_i^P are indeed initially both negative

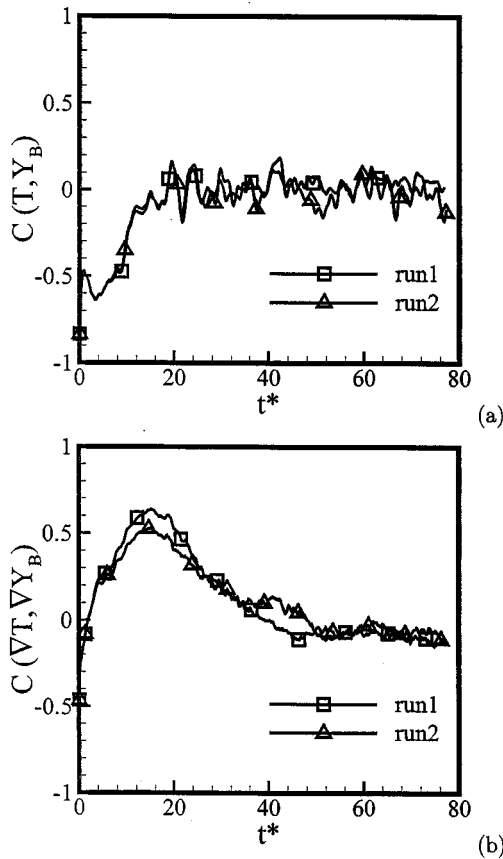


FIG. 5. Temporal evolution of the correlation coefficient between (a) the temperature and heptane mass fraction, and (b) the temperature gradient and the heptane mass fraction gradient.

[see also Fig. 5(b)]. However, this is rapidly reversed (the J_i^T term becomes positive) and the temperature induced Soret diffusion results in a clear opposition to the Fickian term for the variance budget for times $t^* < 20$. The only effect that could change the sign of $\langle J_i^T \partial Y_B / \partial x_j \rangle$ for the present situation would be if the correlation between the temperature and mass fraction gradients were to change sign. This is confirmed in Fig. 5(b) which reveals that this sign change occurs relatively rapidly for both flows, despite the initial lowered temperature of the blob fluid. The correlation coefficient for two vectors a_i and b_i is defined by

$$C(a_i, b_i) = \frac{\langle a_i b_i \rangle}{(\langle a_j a_j \rangle \langle b_k b_k \rangle)^{1/2}}, \quad (22)$$

which is bounded by $-1 \leq C \leq +1$ (no summation is implied on the left-hand side of the above equation). This reversal of correlation occurs at $t^* \approx 2$, again despite the fact that the pure heptane “core” of the blob has not yet been mixed [as evidenced in Fig. 3(a)] and the temperature and mass fraction themselves remain anticorrelated at this time [Fig. 5(a)]. The opposite signs for the two correlations shown in Fig. 5 indicate that although the heptane remains correlated with low temperature fluid regions, regions of large heptane mass fraction gradient generally reside in reduced temperature gradient regions. This occurs for both run 1 and run 2 and therefore cannot be attributed to cross-diffusion

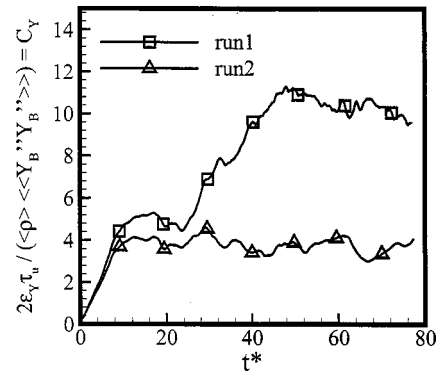


FIG. 6. Temporal evolution of the mechanical to scalar time scale ratio C_Y .

effects. What is occurring is related to the relatively strong density interfaces in regions separating nitrogen and heptane due to their molecular weight difference. It has previously been observed that density interfaces dampen turbulent eddies due to inertial effects.^{36,39} The above results are consistent with a corresponding reduction in temperature gradients along these interfaces.

The above discussion was limited to early mixing times for $t^* < 40$. The latter stages of mixing are highlighted in Fig. 4(b) in which the scalar variance budget is normalized by the instantaneous dissipation values for run 1. In this case, the term due to J_i^Y is by definition equal to negative one, and the remaining terms represent contributions relative to the dissipation term [which itself becomes statistically stationary at long times $t^* > 40$ (see Figs. 3 and 6)]. The long time results depicted in Fig. 4(b) are consistent with the observations of Miller¹⁹ in that an eventual balance is achieved between dissipative effects due to Fickian diffusion and production effects due to the pressure gradient induced Soret diffusion. The temperature gradient induced term represents an insignificant contribution to the long time scalar variance budget. This is the opposite trend from early times in which J_i^T displays a larger magnitude than does J_i^P in the scalar variance budget [Fig. 4(a)].

The long time mixing behavior described above may have direct impact on practical mixing and combustion models. For example, for incompressible flow, exponential variance decay is consistent with an assumption of proportionality between the characteristic scalar decay time scale ($\tau_Y = \frac{1}{2} \rho \langle Y'^2 \rangle / \epsilon_Y$) and the turbulence velocity characteristic time scale ($\tau_u = k / \epsilon_u$; where k is the turbulence kinetic energy and ϵ_u is the velocity dissipation); $\tau_Y = \tau_u / C_Y$, where C_Y is the “mechanical to scalar time scale ratio” taken to be approximately equal to 2.¹ This assumption yields $\epsilon_Y = \frac{1}{2} \rho C_Y \langle Y'^2 \rangle / \tau_u$. Combined with Eq. (5) this yields an analytic solution consistent with exponential variance decay: $\langle Y'^2 \rangle = \langle Y'^2 \rangle_0 \exp(-C_Y \tau^*)$, where $\tau^* = t / \tau_u$ is a nondimensional mixing time. The time scale ratio C_Y finds application in both deterministic⁴⁰ and stochastic^{2,41–43} models for molecular mixing in PDF methods.¹ However, the present results show that exponential variance decay does not occur in the presence of Soret diffusion; the long time scalar variance is stationary [Fig. 3(b)].

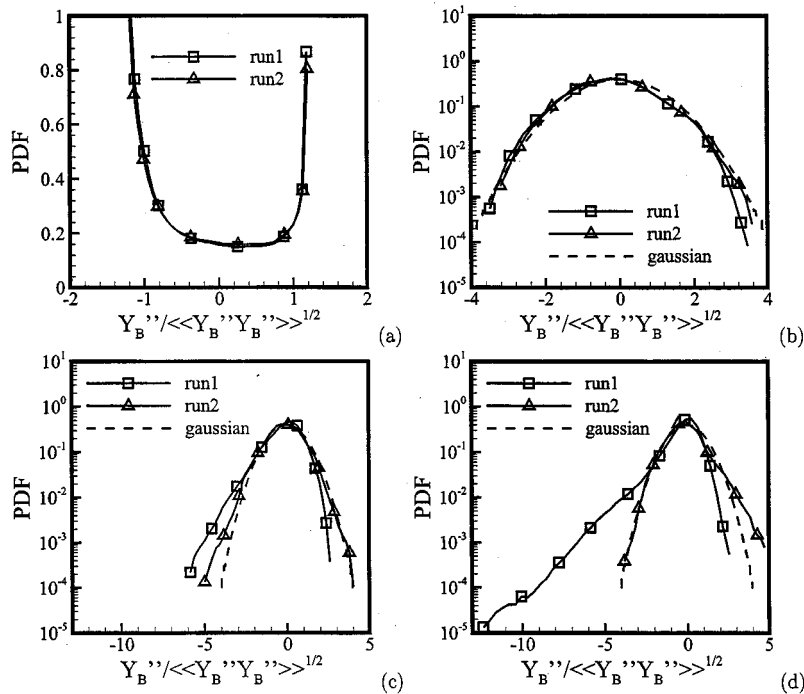


FIG. 7. Probability density function of the normalized heptane mass fraction Favre fluctuations at times (a) $t^* = 5$, (b) $t^* = 20$, (c) $t^* = 40$, and (d) $t^* = 70$.

It should be noted here that the literature suggests both Reynolds number and Schmidt number dependencies for C_Y , as well as possible effects due to initial scalar distributions.²⁷ These influences are all fixed for the present flow simulations and should therefore not obfuscate the following results. The mechanical to scalar time scale ratio, C_Y , is calculated for the present compressible flows as

$$C_Y = \frac{2\epsilon_Y \tau_u}{\langle \rho \rangle \langle Y_B'' Y_B'' \rangle} \tag{23}$$

The turbulence inverse frequency is $\tau_u = k/\epsilon_u$, where the kinetic energy is $k = \frac{1}{2} \langle \rho \rangle \langle u_i'' u_i'' \rangle$, and the velocity dissipation was defined previously. The time scale ratio C_Y calculated from simulations run 1 and run 2 is presented in Fig. 6 as a function of nondimensional time. Simulation run 2 is characterized by an initial transient leading to a stationary value for the ratio, $C_Y \approx 3.5$. This is somewhat larger than the value $C_Y = 2$ suggested by Pope; the difference may be due to compressibility effects inherent to the present flow. In contrast, the C_Y measured for simulation run 1 only follows this trend until $t^* \approx 25$ (with somewhat larger value $C_Y \approx 5$) after which the value of C_Y increases steadily until a new stationary state is achieved with $C_Y \approx 10$. The time of divergence ($t^* \approx 25$) is substantially earlier than the onset of stationary scalar variance at $t^* \approx 40$ [see Fig. 3(b)] due to an enhanced sensitivity of the scalar dissipation to Soret effects [see Fig. 4(b)]. Note in the above that τ_u remains relatively consistent between the two simulations for all times (not shown). Despite the dramatic differences in the curves in Fig. 6, it remains uncertain how significant of an effect would be produced in an actual combustion simulation using the purely Fickian based value of C_Y in conjunction with a standard mixing model due to the fact that a large proportion of the

mixing/reaction will occur prior to the divergence time ($t^* < 25$). Examinations of the scalar PDF and conditional expectations will provide further information in this regard, and the ultimate impact of the results for practical flow modeling will be discussed in the conclusions.

B. Scalar probability density function evolution

The above results indicate the presence of two primary mixing regimes in regard to cross-diffusion effects. The early mixing time regime is characterized by a measurable and significant magnitude for the mass flux vector due to temperature gradients (Fig. 4), but with relatively insignificant alterations to either the scalar bounds or the scalar variance (Fig. 3). In contrast, the long time mixing process is dominated by Soret diffusion due to pressure gradients (J_i^p), resulting in drastic alterations to the behavior of the scalar bounds and variance (which become stationary). The above observations were made with regard to ensemble averaged quantities. Significantly more information is contained within the PDF of the scalar.

Figure 7 presents the single-point single-time PDF of the Favre fluctuations of the heptane mass fraction normalized by their respective standard deviations for both simulations at the times $t^* = 5$, $t^* = 20$, $t^* = 40$, and $t^* = 70$. All PDFs, and the conditional expectations which follow, are computed using 40 bins for the averaging. The PDFs corresponding to the first two times [Figs. 7(a) and 7(b)] reveal the evolution of the scalar distribution from initially segregated (double delta function) to well mixed (asymptotically gaussian) typically observed in previous binary mixing studies.^{27,28} Note that the asymmetry observed in the initial scalar PDF is due to the nonequal density of the heptane and nitrogen. Despite

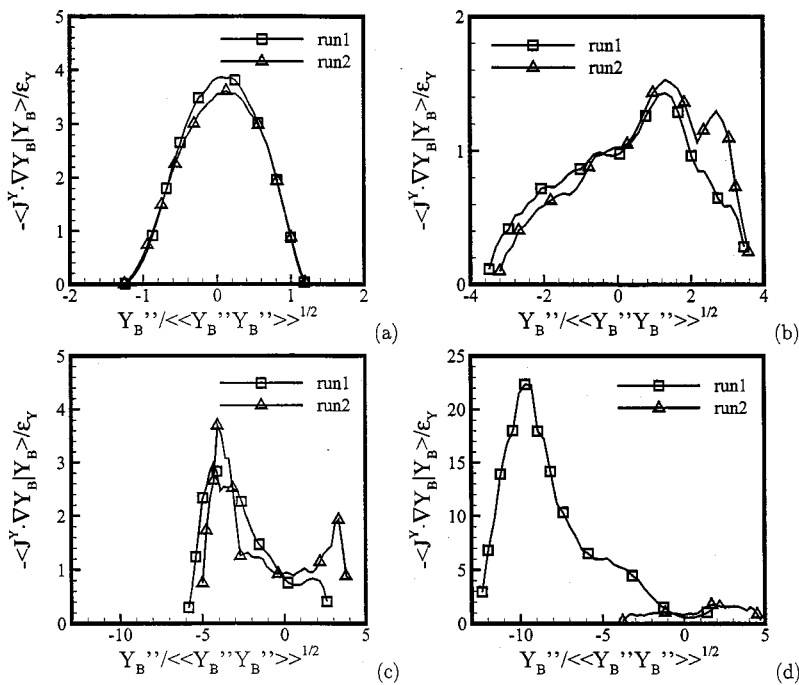


FIG. 8. Expected heptane dissipation conditioned on the Favre mass fraction fluctuation at times (a) $t^* = 5$, (b) $t^* = 20$, (c) $t^* = 40$, and (d) $t^* = 70$.

the alterations to the mass flux terms due to Soret diffusion, the PDFs at these times are indistinguishable between run 1 and run 2. In contrast, by time $t^* = 40$ the migration of the scalar bounds and corresponding decay of the scalar variance have terminated (Fig. 3). While the scalar PDF for run 2 remains approximately gaussian for this and all future times, Soret diffusion begins to skew the PDF at this time towards negative fluctuations. By time $t^* = 70$ the mass fraction PDF for run 1 has become dramatically skewed, with a broad exponential tail extending more than 12 standard deviations

into negative fluctuations. Note that the sign of the skewness is a function of which species is considered; the nitrogen mass fraction PDF displays a positive skewness. Miller¹⁹ observed that the cause of the skewness, and its relation to the particular species, is the partial molar volume difference which appears in the definition of J_i^p . Skewness therefore only becomes prevalent in the scalar PDF at relatively long times when the pressure induced Soret term achieves significant magnitude relative to the remaining scalar variance budget [Fig. 4(b)].

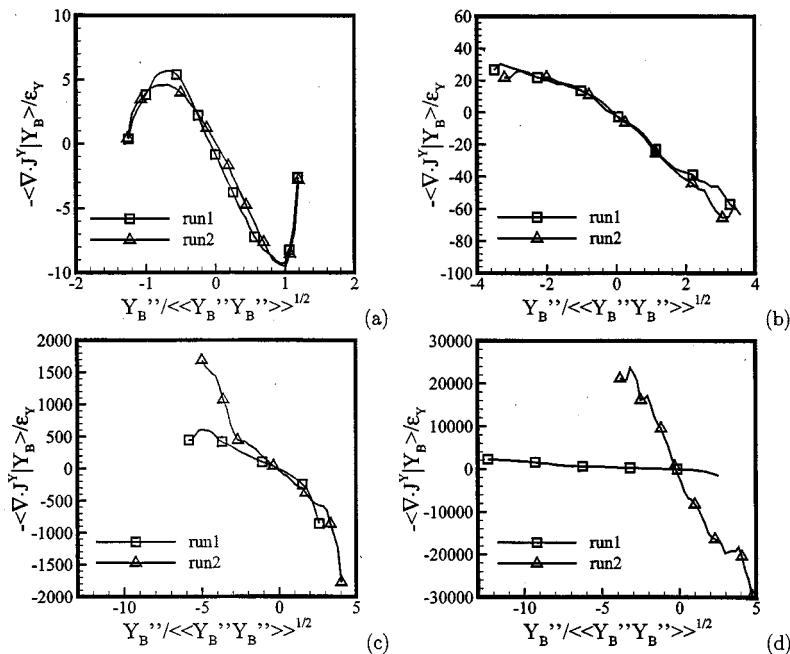


FIG. 9. Expected heptane diffusion conditioned on the Favre mass fraction fluctuation at times (a) $t^* = 5$, (b) $t^* = 20$, (c) $t^* = 40$, and (d) $t^* = 70$.

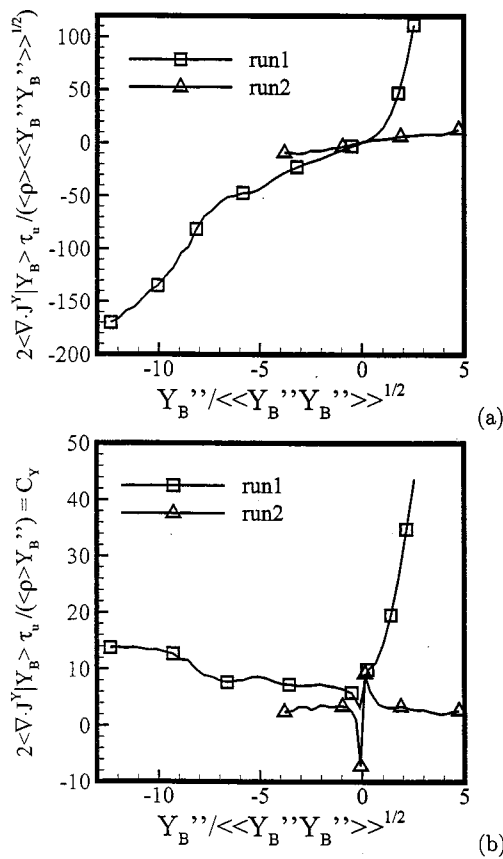


FIG. 10. Expected heptane “dissipation” from pressure and temperature gradient mass flux vectors conditioned on the Favre mass fraction fluctuation at time $t^* = 70$ normalized such that Eq. (24) predicts (a) a linear function with slope C_Y , and (b) a constant equal to C_Y .

C. Conditional expected dissipation and diffusion

The conditional expected scalar dissipation and diffusion provide an alternative measure of the scalar distribution evolution. Furthermore, these terms appear in unclosed form in the PDF transport equation [Eqs. (1) and (2)], and molecular mixing models aim to accurately capture the forms and evolutions of one or the other of these conditional expectations.^{1,28} For the purpose of the present study, the effects of Soret diffusion on the conditional expectations will be gauged through comparisons with those measured for simulation run 2 based on purely Fickian diffusion. In this manner, we only wish to investigate whether or not Soret effects substantially alter the “typical” conditional expectation behavior. We will not at this time attempt to solve the modeled PDF transport equation for *a posteriori* comparisons. The ultimate net effect of any observed Soret effects on the performance of actual combustion models is deferred for future study.

Conditional expectations based on the mass diffusion flux can be analyzed, and/or modeled, by either considering the total flux vector J_i [in the sense of Eqs. (1) and (2)], or by decomposing the flux into separate contributions due to mass fraction (J_i^Y), temperature (J_i^T), and pressure (J_i^P) gradient contributions [in the sense of Eqs. (6) and (7)]. The first approach is somewhat problematic for two related reasons. First, the scalar variance (non-negative) dissipation cannot

be defined based on the total flux vector J_i [see Eq. (9)]. Second, molecular mixing models for PDF methods are based on the relationship between the mass flux and the scalar variance dissipation; i.e. that the conditional dissipation integrates to the mean dissipation [Eq. (3)] and contains the corresponding mixing physics. In light of this we will take the approach of basing the conditional expected dissipation and diffusion only on J_i^Y . The cross-diffusion fluxes, J_i^T and J_i^P , will therefore result in new terms appearing in the scalar PDF transport equation, Eqs. (6) and (7). These new terms will be discussed in the following section.

Figure 8 presents the conditional expected dissipation for both simulations at times $t^* = 5$, $t^* = 20$, $t^* = 40$, and $t^* = 70$. The expectations are normalized by the instantaneous mean Fickian dissipation values, and are conditioned on the scalar Favre fluctuations normalized by their respective standard deviations. The evolution of the expectations in the absence of Soret diffusion (run 2) is consistent with previous observations of the binary mixing process.^{27,28} The expected dissipation begins with a concave downward profile representative of the initially segregated scalars. As the scalar distribution approaches gaussian, the curvature of the core profile switches to concave upward temporarily [Fig. 8(c)], before settling to a near constant valued function indicative of gaussian behavior [Fig. 8(d)].⁴⁴ Asymmetries in the curves are due to the molecular weight difference of the two species.

In the presence of Soret diffusion (run 1), the trends exhibited by the conditional dissipation (based on J_i^Y) are nearly identical at early and intermediate times [Figs. 8(a)–8(c)]. This is not the case at relatively long times for which the scalar distribution has reached its stationary state due to pressure gradient induced Soret effects (see Figs. 3 and 4). Figure 8(d) shows that the conditional dissipation is only consistent with the purely Fickian flow behavior near the core of the scalar distribution and for positive fluctuations. For large negative scalar fluctuation values, the conditional dissipation reaches values in excess of 20 times the mean dissipation value. These peak dissipation events occur at approximately 10 standard deviations from the scalar mean, and correspond to the extended regions of the scalar PDF discussed above [Fig. 7(d)]. This exhibition of large amplitude intermittent dissipation is reversed to the positive scalar fluctuation values for the nitrogen mass fraction conditional expectation. As with the scalar PDF itself, these trends are direct consequences of the production nature of the pressure gradient induced Soret term, J_i^P .

The evolution of the conditional expected diffusion profiles are displayed in a similar manner in Fig. 9 for the same times and normalization as in Fig. 8. The diffusion trends are similar to previous observations for both flows,²⁸ evolving from inverse “cusps” to quasilinear profiles. However, at time $t^* = 70$ the magnitude of the slope is substantially reduced in the presence of Soret diffusion due to its stationary scalar distribution at long times. The normalization with ϵ_Y used in Fig. 9 is somewhat obfuscating in considering the potential impact of this apparent slope change on models for molecular mixing. Models for the conditional diffusion are typically based on an assumption of linear functionality with

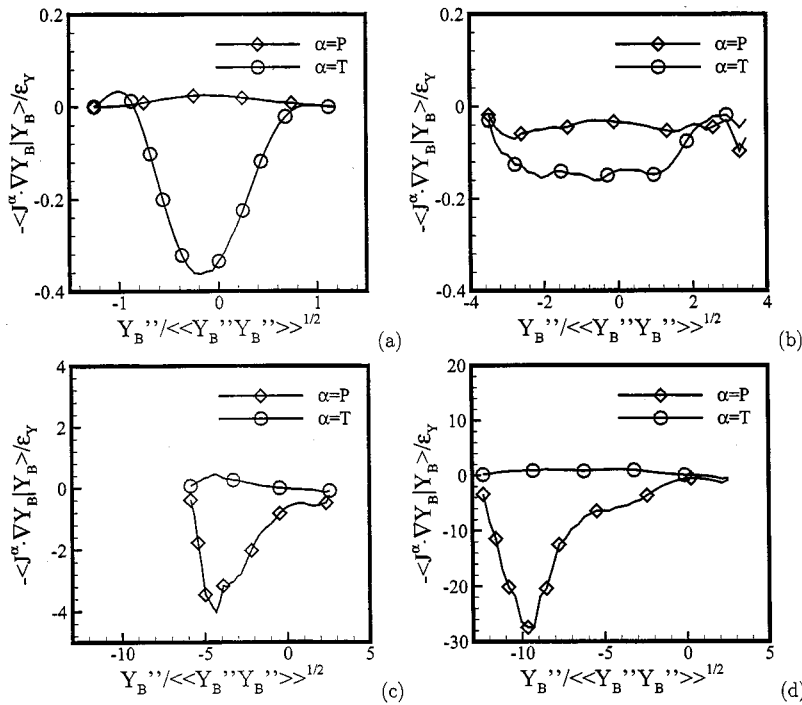


FIG. 11. Expected heptane “dissipation” from pressure and temperature gradient mass flux vectors conditioned on the Favre mass fraction fluctuation at times (a) $t^* = 5$, (b) $t^* = 20$, (c) $t^* = 40$, and (d) $t^* = 70$.

slope as a function of the turbulence velocity time scale and the mechanical to scalar time scale ratio C_Y discussed above. In this regard, the conditional diffusion is not typically normalized with the scalar dissipation itself since it is unknown in general. For example, Dopazo’s model⁴⁰ can be applied to the present flow in the form

$$\frac{2\tau_u}{\langle\rho\rangle} \left\langle \frac{\partial J_i^Y}{\partial x_j} \middle| Y = \psi \right\rangle = C_Y (\psi - \langle\langle Y \rangle\rangle), \quad (24)$$

which is presented in such a form as to yield a linear function with slope equal to C_Y when plotted against the scalar fluctuation ($Y_B'' = Y_B - \langle\langle Y_B \rangle\rangle$). Clearly, this model would predict approximately the same slope for the conditional expected diffusion for both run 1 and run 2, if the same value for C_Y is applied to both flows, since the velocity time scale (τ_u) is essentially unaltered by the Soret diffusion (not shown).

In order to test the functional form assumed in Dopazo’s model, the conditional diffusion at time $t^* = 70$ is presented in Fig. 10 in two manners consistent with Eq. (24) for both simulations. To be fair, Dopazo’s model was of course not originally formulated for use at supercritical pressures. The following results are aimed at both evaluating the model’s performance if applied to these conditions, as well as elucidating the physics of the high pressure mixing process. Figure 10(a) tests the linear dependence suggested by Eq. (24) directly, whereas in Fig. 10(b) the same data are divided by the scalar fluctuation such that the plots should result in a constant value equal to C_Y if the model is correct (the data in both figures are normalized by the scalar standard deviation). The first figure [10(a)] reveals that the data for run 2 are consistent with the linear model prediction. However, run 1 is characterized by two regions of markedly differing slope corresponding to the positive and negative scalar fluctua-

tions. The predicted proportionality ratio in Fig. 10(b) is nearly constant valued for all scalar fluctuations for run 2, with $C_Y \approx 3.5$ consistent with Fig. 6 (except for the region near $Y_B'' = 0$ where the term is singular). On the other hand, in the presence of Soret diffusion the simulation data (run 1) do not yield a constant valued function. Figure 6 showed that the ratio of time scales (C_Y) does achieve a stationary value at long times for run 1. Therefore, the present results [Fig. 10(b)] suggest that it is the model form in Eq. (24) itself which is inconsistent with the long time conditional diffusion behavior in the presence of Soret cross diffusion. As mentioned above, the ultimate effect of modeling inadequacies at these times on the overall accuracy of PDF methods cannot be determined satisfactorily without further *a posteriori* testing, due to the fact that the majority of combustion will have already occurred prior to these relatively late times.

D. Cross-diffusion conditional expectations

The evolutions of the four new conditional expectations due to Soret cross diffusion which appear in Eqs. (6) and (7) are presented in Figs. 11 and 12. The conditional “dissipation” terms due to J_i^T and J_i^P [Eq. (6)] are depicted in Fig. 11, whereas the corresponding conditional “diffusion” terms [Eq. (7)] are shown in Fig. 12. Note, the terms “dissipation” and “diffusion” are only used loosely in the above. These processes only have similar forms to the Fickian dissipation and diffusion terms, but do not physically satisfy the definitions of the respective processes. For example, the conditional “dissipation” in Fig. 11 can exhibit both positive and negative values corresponding to either a dissipation or a production process. For the present flow, both J_i^T and J_i^P act primarily as production terms at all times (Fig. 11). Consistent with the above observations, at early times the tempera-

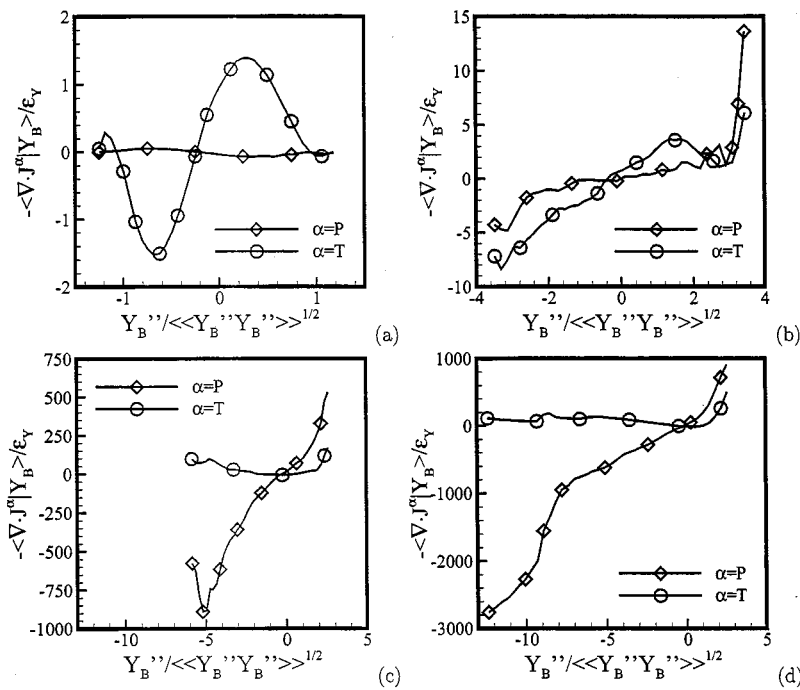


FIG. 12. Expected heptane “diffusion” from pressure and temperature gradient mass flux vectors conditioned on the Favre mass fraction fluctuation at times (a) $t^* = 5$, (b) $t^* = 20$, (c) $t^* = 40$, and (d) $t^* = 70$.

ture gradient based term J_i^T dominates the Soret effects due to substantially larger temperature gradients in the early flow (although the net effect on the scalar variance evolution is relatively minor at these times). In contrast, at long times after the initial cold heptane blob has been mixed and the scalar achieves its stationary state the pressure based term dominates. At these times, the pressure gradient induced Soret diffusion acts as a production mechanism concentrated in the large negative heptane fluctuations [Fig. 11(d)], with nearly equal and opposite magnitude relative to the Fickian dissipation term [Fig. 8(d)].

Note that by time $t^* = 70$ the scalar PDF has reached a nearly stationary form, and the terms in Figs. 11(d) and 12(d) approximately cancel the corresponding Fickian based dissipation and diffusion shown in Figs. 8(d) and 9(d), respectively. This effectively nulls the right-hand side of the PDF transport equation [Eqs. (6) and (7)], yielding a stationary scalar distribution. This is also why it is inappropriate to apply previous mixing models, such as Dopazo’s [Eq. (24)], to the total mass flux vector, $J_i = J_i^Y + J_i^T + J_i^P$. Such models predict a conditional diffusion dependent only on the mechanical to scalar time scale ratio and the turbulence time scale consistent with continuous scalar variance decay. They are presently incapable of predicting the stationary scalar PDFs exhibited in the presence of cross diffusion. Even if Dopazo’s model were found to adequately model the Fickian conditional diffusion (due to J_i^Y), the conditional “diffusion” terms resulting from J_i^T and J_i^P would still require modeling in order to capture the long time stationary scalar distribution.

IV. CONCLUSIONS

Direct numerical simulations have been conducted for the binary mixing problem in isotropic compressible turbu-

lence at supercritical pressure. Two simulations at resolutions of 192^3 grid points were conducted for the study. Both cases correspond to mixing of initially segregated heptane in nitrogen (50/50 by mass) at 45 atm mean pressure and 700 K mean temperature. The heptane is initially in the form of a spherical “blob” of fluid cooled by 50 K relative to the surrounding nitrogen in order to model effects of temperature stratification found with cold fuel injection systems. The turbulence is characterized by a mean Taylor based Reynolds number $Re_\lambda \approx 80$ and a mean fluctuation Mach number $M_C \approx 0.54$. The only difference between the two simulations is that in one case the complete generalized diffusion fluxes derived from nonequilibrium thermodynamics and fluctuation theory are employed. As a basis for comparisons, the second simulation employs only the “standard” Fickian and Fourier diffusion. Both cases incorporate a cubic Peng–Robinson real gas state equation.

The results are analyzed in the context of *a priori* evaluations of probability density function (PDF) methods for extension to supercritical pressure flow situations. At early mixing times prior to the destruction of the heptane blob, cross diffusion due to temperature gradients has a measurable productive impact on the scalar variance transport equation. However, for the present isotropic mixing problem, any imposed temperature gradient surrounding the heptane blob is quickly deteriorated by the turbulence, thus limiting the associated cross-diffusion effects. Therefore, at early times prior to the destruction of the heptane blob, the evolution of the scalar PDF and related statistics is relatively unaffected by the presence of Soret diffusion. It is, however, important not to draw general conclusions concerning early time mixing behavior from these observations. Some flow situations inherently involve large magnitude persistent temperature gradients which may alter these above conclusions.

For example, Miller *et al.*³⁶ studied a temperature stratified mixing layer and found relatively large effects due to the temperature induced Soret diffusion at all times.

In contrast to early times, during the latter stages of mixing the scalar distribution is found to be markedly altered in the presence of Soret diffusion. It is observed that pressure gradient induced cross-diffusion acts as a production mechanism in the scalar variance equation. As the mixing proceeds, and the variance decays, an eventual balance is reached between this production effect and dissipation due to the Fickian diffusion term. At sufficiently long times, the scalar variance reaches a statistically stationary value in the presence of Soret diffusion. It is shown that the application of standard PDF models may be severely impeded at these times. For example, the mechanical to scalar time scale ratio, $C_Y = \tau_u / \tau_Y$, is increased by a factor of approximately 3 relative to that measured in the absence of cross diffusion. The scalar PDF itself is shown to become highly skewed with exponentially decreasing tail well beyond 10 standard deviations from the mean scalar value. The conditional expected scalar Fickian dissipation exhibits very large amplitude values for these negative scalar fluctuations, which are balanced at long times by the productive effect of the conditional “dissipation” due to pressure gradients. Dopazo’s molecular mixing model⁴⁰ for the conditional expected diffusion is tested for the present high pressure mixing problem. The functional form is observed to be inconsistent with the DNS data in the presence of cross diffusion at long mixing times.

Despite the apparently substantial effects of Soret diffusion on the long time scalar distribution and evolution, it remains to be determined how significant an impact is to be expected in actual PDF model applications to high pressure turbulent reacting flows. The scalar variance has substantially decayed before Soret effects are measured to be important, and the majority of combustion would have already occurred prior to this time. On the other hand, accurate prediction of flame temperatures and product species concentrations may prove sensitive to these long time flow conditions. Some flows, such as jets, will involve regions of well mixed fluid (jet center) under persistent interaction with the large reaction rate regions (jet edges and vortical structures). Other flow situations, such as mixing layers, will involve mean imposed temperature gradients which could make Soret effects important even at early times. Local flames are obviously also characterized by large temperature gradients which may enhance Soret diffusion effects to important levels even at early times. Although limited to binary mixing in isotropic turbulence, the present investigation has elucidated the mechanisms by which nonequilibrium cross diffusion can potentially impact standard PDF modeling of turbulent mixing and combustion, and has suggested a need for further research in this area.

ACKNOWLEDGMENTS

This research was supported by the National Science Foundation through the Faculty Early Career Development Program; Grant No. CTS-9983762. Computational support

was provided by the California Institute of Technology’s Center for Advanced Computing Research (CACR) utilizing the Hewlett-Packard V2500.

- ¹S. B. Pope, “PDF methods for turbulent reacting flows,” *Prog. Energy Combust. Sci.* **11**, 119 (1985).
- ²C. Dopazo and E. E. O’Brien, “Statistical treatment of non-isothermal chemical reactions in turbulence,” *Combust. Sci. Technol.* **13**, 99 (1976).
- ³P. R. Van Slooten, Jayesh, and S. B. Pope, “Advances in PDF modeling for inhomogeneous turbulent flows,” *Phys. Fluids* **10**, 246 (1998).
- ⁴B. J. Delarue and S. B. Pope, “Application of PDF methods to compressible flows,” *Phys. Fluids* **9**, 2704 (1997).
- ⁵B. J. Delarue and S. B. Pope, “Calculations of subsonic and supersonic turbulent reacting mixing layers using probability density function methods,” *Phys. Fluids* **10**, 487 (1998).
- ⁶M. Zhu, K. N. Bray, O. Rumberg, and B. Rogg, “PDF transport equations for two-phase reactive flows and sprays,” *Combust. Flame* **122**, 327 (2000).
- ⁷R. V. R. Pandya and F. Mashayek, “Probability density function modeling of evaporating droplets dispersed in isotropic turbulence,” *AIAA Paper* 2001-0333 (2001).
- ⁸O. E. Tewfik, E. R. G. Eckert, and C. J. Shirliff, “Thermal diffusion effects on energy transfer in a turbulent boundary layer with helium injection,” *Proceedings of the 1962 Heat Transfer and Fluid Mechanics Institute*, 1962, pp. 42–61.
- ⁹O. E. Tewfik and J. W. Yang, “The thermodynamic coupling between heat and mass transfer in free convection with helium injection,” *Int. J. Heat Mass Transf.* **6**, 915 (1963).
- ¹⁰E. M. Sparrow and E. R. G. Minkowycz, “Diffusion-thermo effects in stagnation-point flow of air with injection of gases of various molecular weights into the boundary layer,” *AIAA J.* **2**, 652 (1964).
- ¹¹E. M. Sparrow, E. R. G. Minkowycz, and W. E. Eckert, “The effect of diffusion thermo and thermal diffusion for helium injection into plane and axisymmetric stagnation flow of air,” *J. Heat Transfer* **86**, 311 (1964).
- ¹²E. M. Sparrow, E. R. G. Minkowycz, and W. E. Eckert, “Transpiration-induced buoyancy and thermal diffusion—Diffusion thermo in a helium-air free convection boundary layer,” *J. Heat Transfer* **86**, 508 (1964).
- ¹³R. L. Mahajan and C. Wei, “Soret, Dufour, and variable property effects in silicon epitaxy,” *J. Heat Transfer* **113**, 688 (1991).
- ¹⁴E. W. Curtis and P. V. Farrell, “A numerical study of high-pressure droplet vaporization,” *Combust. Flame* **90**, 85 (1992).
- ¹⁵S. D. Givler and J. Abraham, “Supercritical droplet vaporization and combustion studies,” *Prog. Energy Combust. Sci.* **22**, 1 (1996).
- ¹⁶K. G. Harstad and J. Bellan, “Isolated fluid oxygen drop behavior in fluid hydrogen at rocket chamber pressures,” *Int. J. Heat Mass Transf.* **41**, 3537 (1998).
- ¹⁷K. G. Harstad and J. Bellan, “Interactions of fluid oxygen drops in fluid hydrogen at rocket chamber pressures,” *Int. J. Heat Mass Transf.* **41**, 3551 (1998).
- ¹⁸K. G. Harstad and J. Bellan, “An all pressure fluid-drop model applied to a binary mixture: Heptane in nitrogen,” *Int. J. Multiphase Flow* **26**, 1675 (2000).
- ¹⁹R. S. Miller, “Long time mass fraction statistics in stationary compressible isotropic turbulence at supercritical pressure,” *Phys. Fluids* **12**, 2020 (2000).
- ²⁰L. B. Benano-Melly, J. P. Caltagirone, B. Faissat, F. Montel, and P. Costesque, “Modeling Soret coefficient measurement experiments in porous media considering thermal and solutal convection,” *Int. J. Heat Mass Transf.* **44**, 1285 (2001).
- ²¹T. S. Lundgren, “Model equation for nonhomogeneous turbulence,” *Phys. Fluids* **12**, 485 (1969).
- ²²C. Dopazo and E. E. O’Brien, “Functional formulation of nonisothermal turbulent reactive flows,” *Phys. Fluids* **17**, 1968 (1975).
- ²³S. B. Pope, “The probability approach to modelling of turbulent reacting flows,” *Combust. Flame* **27**, 299 (1976).
- ²⁴G. Kosaly and P. Givi, “Modeling of turbulent molecular mixing,” *Combust. Flame* **70**, 101 (1987).
- ²⁵S. B. Pope, “Computations of turbulent combustion: Progress and challenges,” *Proceedings of the 23rd Symposium (International) on Combustion*, 1990, pp. 591–612.
- ²⁶S. B. Pope, “Mapping closures for turbulent mixing and reaction,” *Theor. Comput. Fluid Dyn.* **2**, 255 (1991).
- ²⁷V. Eswaran and S. B. Pope, “Direct numerical simulations of the turbulent

- mixing of a passive scalar," *Phys. Fluids* **31**, 506 (1988).
- ²⁸R. S. Miller, S. H. Frankel, C. K. Madnia, and P. Givi, "Johnson–Edgeworth translation for probability modeling of binary mixing in turbulent flows," *Combust. Sci. Technol.* **91**, 21 (1993).
- ²⁹B. Castaing, G. Gunaratne, F. Heslot, L. Kadanoff, A. Libchaber, S. Thomae, X. Z. Wu, S. Zaleski, and G. Zanetti, "Scaling of hard thermal turbulence in Rayleigh–Benard convection," *J. Fluid Mech.* **204**, 1 (1989).
- ³⁰C. Tong and Z. Warhaft, "Passive scalar dispersion and mixing in a turbulent jet," *J. Fluid Mech.* **292**, 1 (1995).
- ³¹F. A. Jaber, R. S. Miller, C. K. Madnia, and P. Givi, "Non-gaussian scalar statistics in homogeneous turbulence," *J. Fluid Mech.* **313**, 241 (1996).
- ³²S. R. De Groot and P. Mazur, *Non-Equilibrium Thermodynamics* (Dover, New York, 1984).
- ³³R. C. Reid, J. M. Prausnitz, and B. E. Poling, *The Properties of Gases and Liquids* (McGraw-Hill, Boston, MA, 1989).
- ³⁴J. Keizer, *Statistical Thermodynamics of Nonequilibrium Processes* (Springer-Verlag, New York, 1987).
- ³⁵S. Sarman and D. J. Evans, "Heat flow and mass diffusion in binary Lennard-Jones mixtures," *Phys. Rev. A* **45**, 2370 (1992).
- ³⁶R. S. Miller, K. G. Harstad, and J. Bellan, "Direct numerical simulation of supercritical fluid mixing layers applied to heptane–nitrogen," *J. Fluid Mech.* **436**, 1 (2001).
- ³⁷S. Kida and S. A. Orszag, "Energy and spectral dynamics in forced compressible turbulence," *J. Sci. Comput.* **5**, 85 (1990).
- ³⁸C. A. Kennedy and M. H. Carpenter, "Several new numerical methods for compressible shear-layer simulations," *Appl. Numer. Math.* **14**, 397 (1994).
- ³⁹I. A. Hannoun, H. J. S. Fernando, and E. J. List, "Turbulence structure near a sharp density interface," *J. Fluid Mech.* **189**, 189 (1988).
- ⁴⁰C. Dopazo, "Probability density function approach for a turbulent axisymmetric heated jet. Centerline evolution," *Phys. Fluids* **18**, 397 (1975).
- ⁴¹R. L. Curl, "Dispersed phase mixing: I. Theory and effects in simple reactors," *AIChE J.* **9**, 175 (1963).
- ⁴²J. Janicka, W. Kolbe, and W. Kollmann, "Closure of the transport equation for the probability density function of turbulent scalar field," *J. Non-Equil. Thermodyn.* **4**, 47 (1979).
- ⁴³S. B. Pope, "An improved turbulent mixing model," *Combust. Sci. Technol.* **28**, 131 (1982).
- ⁴⁴F. A. Jaber, R. S. Miller, and P. Givi, "Conditional statistics in turbulent scalar mixing and reaction," *AIChE J.* **42**, 1149 (1996).